EFFECTS OF NANOPARTICLE VOLUME FRACTION IN HYDRODYNAMIC AND THERMAL CHARACTERISTICS OF FORCED PLANE JET

by

Mohammad Javad MAGHREBI [a], ***Taher ARMAGHANI*** [b*], ***and Farhad TALEBI*** [c]

[a] Mechanical Engineering Department, Ferdowsi University of Mashhad, Mashhad, Iran
[b] Islamic Azad University Mahdishahr Branch, Department of Engineering, Mahdishahr, Iran
[c] Mechanical Engineering Department, Semnan University, Semnan, Iran

Original scientific paper
DOI: 10.2298/TSCI101011022M

The effects of nanoparticle volume fraction in hydrodynamic and thermal characteristics of an incompressible forced 2-D plane jet flow are investigated. Direct numerical simulation of a 2-D incompressible plane forced jet flow for two nanofluids has been performed. The base fluid is water and the nanoparticles are Al_2O_3 and CuO. The numerical simulation is carried out for the solid volume fraction between 0 to 4%. The results for both nanofluids indicate that any increase in the solid volume fraction decreases the amplitude of temperature, velocity time histories, the turbulent intensities, and that of the Reynolds stresses. The results for both two nanoparticles also indicate that with any increase in nanoparticle volume fraction, the velocity amplitude of velocity time history, the turbulent intensities, and Reynolds stress in Al_2O_3-water are greater than that of CuO-water nanofluid.

Key words: *incompressible plane jet, nanoparticle volume fraction, velocity time history, temperature time history, turbulent intensities, Reynolds stress*

Introduction

Nanofluids, a name conceived by Choi [1] in Argonne National Laboratory, are fluids consisting of solid nanoparticles with sizes less than 100 nm suspended in with solid volume fraction typically less than 4%.

Nanofluids can enhance heat transfer performance compared with pure liquids. Nanofluids can be used to improve thermal management system in many engineering application such as nanofluid in transportation, micromechanics, instrument, HVAC, and cooling system [2].

Recently, many investigators studied the nanofluid convective heat transfer in different geometries both numerically and experimentally. Maiga *et al.* [3, 4] numerically investigated the hydrodynamic and thermal characteristics of nanofluids flowing through a uniformly heated tube in both laminar and turbulent regimes. They showed that the addition of nanoparticle can increase the heat transfer substantially compared with the base fluid alone. In

* Corresponding author; e-mail: taherarmaghani@yahoo.com

other study, Maiga *et al.* [5] proposed a new correlation to describe the thermal performance of Al_2O_3-water nanofluids under turbulent regime. There are many numerical and experimental investigations about nanofluid thermal and hydrodynamic behavior in tubes and annulus [6-12]. A numerical investigation of laminar mixed convection flow through a copper-water nanofluid in a square lid-driven cavity has been studied by Talebi *et al.* [13]. They showed the effect of solid concentration as a positive effect on heat transfer enhancement.

A numerical investigation of mixed convection flows through a copper-water nanofluid in a square cavity with inlet and outlet port has been performed by Shahi *et al.* [14]. The results indicated that any increase in solid concentration leads to an increase in the average Nusselt number at the heat source surface and a decrease in the average bulk temperature.

The effectiveness assessment of Al_2O_3 nanoparticle at enhancing single-phase and two-phase heat transfer in micro-channel heat sinks has been performed by Lee *et al.* [15]. They found that the high thermal conductivity of nanoparticles were enhanced the single-phase heat transfer coefficient. However, the enhancement was found weaker in a fully developed region. It was proved that nanoparticles had an important effect on thermal boundary layer development.

The heat transfer due to laminar flow of copper-water nanofluid through two isothermally heated parallel plates was studied by Santra *et al.* [16]. They considered the fluid as Newtonian as well as non-Newtonian for a wide range of Reynolds and solid volume fraction. The results indicated that the rate of heat transfer increased with an increase in flow as well as an increase in solid volume fraction of the nanofluid. Unlike natural convection, the heat transfer was increased for both cases.

The study of confined and submerged impinging jet heat transfer using Al_2O_3-water nanofluid has been investigated experimentally by Nguyen *et al.* [17]. They reported that the use of nanofluid can provide a clear heat transfer enhancement for both laminar and turbulent regime. It has also been found that nanofluids with high particle fraction were not appropriate for the heat transfer enhancement purpose under the configuration of confined and submerged impinging jet.

In this work we study the effects of nanoparticle volume fraction in a hydrodynamic and thermal characteristic of a forced plane jet, which has a wide range of application in fusion [18, 19], vacuum environment [20], and cooling of electronic devices.

The effective thermal conductivity of nanofluid has been calculated with a model proposed by Yu *et al.* [21].

To determine the viscosity of nanofluid, we used two experimental correlations for Al_2O_3-water and CuO-water nanofluids proposed by Nguyen *et al.* [22].

The governing equations

Figure 1 shows the co-ordinate system and the computational domain in which the governing equation for the incompressible jet flow are solved. The inlet velocity profile is specified by $U_0(y)$ that has a superimposed computational velocity. The jet flow is allowed to develop in the spatial x-direction.

In this paper the governing equations are derived from the full incompressible Navier-Stokes and energy equations. These equations together with an equation representing mass conservation are the governing equation for an incompressible plane jet flow. These are solved in a domain which is finite in the streamwise x-direction and doubly infinite in the cross--stream y-direction. In x-direction a high order compact finite difference scheme is used. In y, the cross-stream direction, a mapped compact finite difference method is employed. All equations are made non-dimensional by appropriate characteristic scales of jet flow. All lengths are normalized by the inlet jet half width, $b_{1/2}$, and velocities are normalized by U_0. The time is normalized by $b_{1/2}/U_0$ and temperature is normalized as $T^* = (T - T_\infty)/(T_0 - T_\infty)$.

The mean component of the streamwise velocity at the inlet plane of the domain, as presented by Schlichting [23], was:

$$U_0(y) = \frac{1}{\cosh^2 y} \tag{1}$$

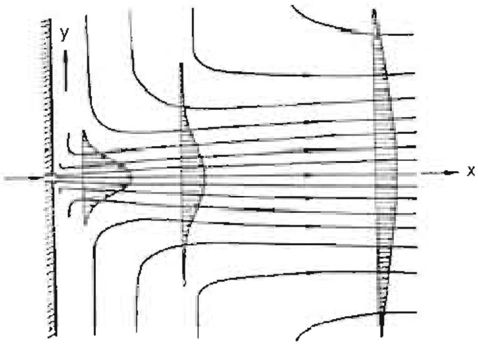

Figure 1. Spatially developing jet geometry

The inlet temperature profile is also assumed the same as the inlet velocity profile. The rotational form of Navier-Stokes equation is:

$$\frac{\partial \nabla^2 \vec{\mathrm{U}}}{\partial t} = -\nabla \times (\nabla \times \vec{\mathrm{H}}) + \frac{1}{\mathrm{Re}} \nabla^4 \vec{\mathrm{U}} \tag{2}$$

where the vector $\vec{\mathrm{H}}(H_1, H_2, H_3) = \vec{\mathrm{U}} \times \vec{\omega}$ contains the non-linear and $1/\mathrm{Re} = \mu/\rho U_{\mathrm{in}} b_{1/2}$. Equation (2), which is obtained by applying the gradient operation, ∇, on the sides of Navier-Stokes equation twice in succession, is the evolution equations responsible for the time-advancement of the simulation.

The instantaneous velocity $\vec{\mathrm{U}} = (U, V)$ is decomposed into a base flow, $\vec{\mathrm{U}}_0(y), 0$, and the computational velocity components, $u(x, y, t)$, $v(x, y, t)$, as:

$$U(x, y, t) = U_0(y) + u(x, y, t) \tag{3}$$

$$V(x, y, t) = v(x, y, t) \tag{4}$$

Using the streamwise components of eq. (2) and the decomposition shown by eq. (3) yields:

$$\frac{\partial}{\partial t} \nabla^2 u = \frac{\partial^2 H_1}{\partial y^2} - \frac{\partial^2 H_2}{\partial x \partial y} + \frac{1}{\mathrm{Re}} \nabla^4 U \tag{5}$$

where $\omega_1 = \omega_2 = H_3 = 0$ for the case of 2-D flow. The cross-stream velocity component v is recovered directly from the continuity equation:

$$\frac{\partial v}{\partial y} = -\frac{\partial u}{\partial x} \tag{6}$$

The vorticity component ω_3 is calculated following its definition:

$$\omega_3 = \frac{\partial V}{\partial x} - \frac{\partial U}{\partial y} \tag{7}$$

Then the energy equation is solved.

$$\frac{\partial T}{\partial t} + \vec{\mathrm{U}} \cdot (\nabla T) = \frac{1}{\mathrm{Pe}} (\nabla^2 T) \tag{8}$$

The instantaneous temperature T is decomposed into a base temperature, $T_0(y)$, and the computational temperature components, $T_c(x, y, t)$, as:

$$T(x, y, t) = T_0(y) + T_c(x, y, t) \tag{9}$$

Boundary and initial conditions

Equation (5) is a fourth-order partial differential equation, so it requires four boundary conditions. The u velocity is specified at the inlet ($x = 0$) and the outlet boundaries ($x = L_x$). With the help of continuity equation, $\partial u/\partial x$ is also specified at the inflow and outflow boundaries:

$$\frac{\partial v}{\partial y} = -\frac{\partial u}{\partial x} \tag{10}$$

The former and the latter are known as Dirichlet and Neumann type boundary conditions, respectively. The boundary conditions are set to zero in the transverse direction.

In the numerical simulation, the instantaneous velocity components at the inlet boundary are specified using cosine hyperbolic profile, eq. (1), which is superimposed by some perturbations.

Convective outflow boundary conditions are specified at the outflow. The boundary condition must be non-reflective to avoid feedback problem. The convective boundary conditions, eq. (11), are used to generate the Dirichlet boundary condition for both velocity components and temperature.

$$\frac{\partial \psi}{\partial t} = -c\frac{\partial \psi}{\partial x} \tag{11}$$

where ψ is replaced by each of the velocity components and temperature. In eq. (11) , c represents the local advection speed of the large-scale structures in the layer at the vicinity of the outlet. That is the local speed of convection at the outlet boundary. This condition allows the flow structures to wash out of the domain in a natural manner. The convective outflow boundary condition was used by many investigators [24-27].

Energy equation requires two temperature boundary conditions, known as Dirichlet boundary conditions. For the forced jet simulation, only the perturbation part for v is excited at the inflow boundary as:

$$v(x, y, t) = A\sin(\omega t) \tag{12}$$

The amplitude and frequency are set to $A = 0.01$ and $\omega = 0.5$, respectively.

A uniformly distributed cosine hyperbolic mean velocity at all x stations is the initial condition. These initial conditions must then be allowed to wash out of the outlet boundary before performing any statistical analysis on the jet flow. In other words, any particle at the inlet ($x = 0$) must be allowed to leave the outlet boundaries ($x = L_x$).

Initial condition for temperature is assumed the same as the velocity initial condition.

Numerical formulation

The spatially developing jet is solved in a domain with a finite extend in the streamwise direction and doubly infinite ($y \rightarrow \pm\infty$) in the major-gradient (MG) direction. A mapping is employed to convert the doubly-infinite y extend of the original domain into a computational domain of ζ with interval $0 \leq \zeta \leq 1$.

The derivatives in the streamwise direction are computed using the Pade' finite difference scheme developed by Lele [28].

The compact finite difference scheme is an implicit scheme, hence the highest order of accuracy can be obtained at the maximum distance from both boundaries where the lower order schemes are used a cotangent mapping given by:

$$y = -\lambda \operatorname{cotg}(\pi\zeta) \tag{13}$$

which is used to map the doubly infinite physical domain $-\infty \leq y \leq \infty$ into the finite computational domain with the interval of $0 \leq \zeta \leq 1$. λ in eq. (13) is a stretching parameter of the mapping. Equation (6) is the governing equation for the cross-stream velocity. Compact finite difference scheme, is subjected to the ill-conditioning problem. To overcome ill-conditioning problem the y derivative operator is applied on the both sides of eq.(6):

$$\frac{\partial^2 v}{\partial y^2} = -\frac{\partial^2 u}{\partial x \partial y} \tag{14}$$

Equation (14) is not ill-conditioned. This also satisfies the boundary conditions at infinites. In other words eq. (14), which is a second order differential equation, is solved using $v(\pm\infty) = 0$ as boundary conditions. A compact third order Runge-Kutta time differencing scheme developed by Wray *et al.* [29] is used to advance the computations in time.

Code verification

To evaluate the code an asymptotical solution correspond to inviscid flow, known as stuart solution, is examined. Stuart [30] provides a class of exact solution to the inviscid Navier-stoks equations which study the 2-D jet flow. The particular solution of interest here has a hyperbolic tangential profile for the u velocity component. As a consequence, the flow is periodic in x-direction and advects downstream at the main speed of the layer, c. The analytical expression for the stream function, ψ, is:

$$\psi(x, y, t) = cy + \ln(a\cosh(y - y_0) + b\cos(x - ct)]$$

where $b = (a^2 - 1)^{1/2}$. The velocity component u and v, as well as the vorticity component ω_z, are obtained by differentiating this expression with respect to x and y as appropriate. They are:

$$u = \frac{\partial \psi}{\partial y} = c + \frac{a\sinh(y - y_0)}{a\cosh(y - y_0) + b\cos(x - ct)} \tag{15}$$

$$v = -\frac{\partial \psi}{\partial x} = \frac{b\sinh(x - ct)}{a\cosh(y - y_0) + b\cos(x - ct)} \tag{16}$$

$$\omega_z = \frac{1}{[a\cosh(y - y_0) + b\cos(x - ct)]^2} \tag{17}$$

The Stuart solution provide an excellent test for the time advancement the formation of the right hand side of eq. (5) and the advection section of the code. Therefore, the time development of this filed was computed for a case with $b = 1/2$ and $c = 1$ on the domain of $0 \leq x \leq L_x = 2\pi/3$ and $-\infty \leq y \leq \infty$. The domain was discretized using $Nx = 45$, $Ny = 40$, and $\lambda = 3$.

Plots of the maximum errors between the numerical result and exact solution of and are shown in fig. 2.

In another asymptotical case the base fluid is applied in which the volume fraction is zero. The dimensionless axial velocity is compared to analytical results of Tollmien [see in 31], Goetler [see in 31], Zijnen's Gaussian profile [32], a sech^2 profile of Thorne [33] and more re-

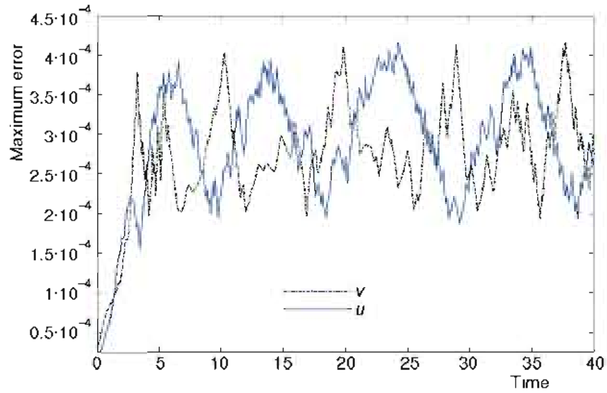

Figure 2. Error analysis for *u* and *v* in time dependant Stuart solution test case

cent analytical expressions of Morchain *et al.* [34] and Aziz *et al.* [35]. As shown in fig. 3 the result is closely fitted with the previous investigations.

Finally in order to ensure the accuracy as well as the consistency of numerical results, a different number of non-uniform grids have been submitted to an extensive testing procedure. The results are obtained for Re = 100 and Pr = 3. Figures 4, 5, and 6 show grid study independencies for *U*, *V*, and *T*. The convergence is achieved for 140 × 70 grid points.

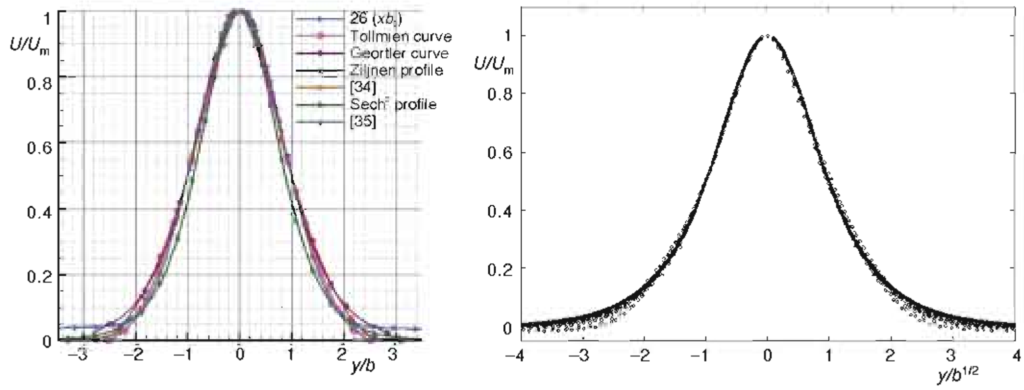

Figure 3. Axial dimensionless velocity; (a) theoretical and experimental results of pervious investigations, (b) present work (color image see on our web site)

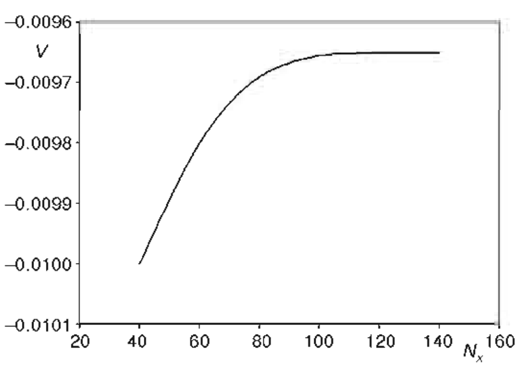

Figure 4. *V* grid sensitivity study at $x = 0.75\ L_x$, $y = 0$, and $t = 100$

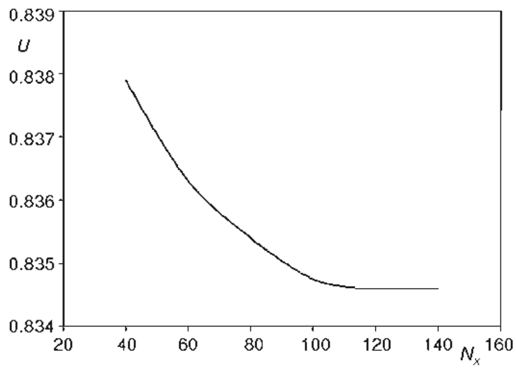

Figure 5. *U* grid sensitivity study at $x = 0.75\ L_x$, $y = 0$ and $t = 100$

Nanofluid mathematical formulation

A single phase, mixture model is used for nanofluids. As mentioned before, many researchers such as Talebi [13, 14 and 36] have examined this model and report a good agreement with experimental data. Using an effective value for thermophysical properties, the momentum and energy equations are written as:

$$\frac{\partial \nabla^2 \vec{\mathrm{U}}}{\partial t} = -\nabla \times (\nabla \times \vec{\mathrm{H}}) + \frac{1}{\mathrm{Re}_{\mathrm{nf}}} \nabla^4 \vec{\mathrm{U}} \quad (18)$$

$$\frac{\partial T}{\partial t} + \vec{\mathrm{U}}(\nabla T) = \frac{1}{\mathrm{Pe}_{\mathrm{nf}}} (\nabla^2 T) \quad (19)$$

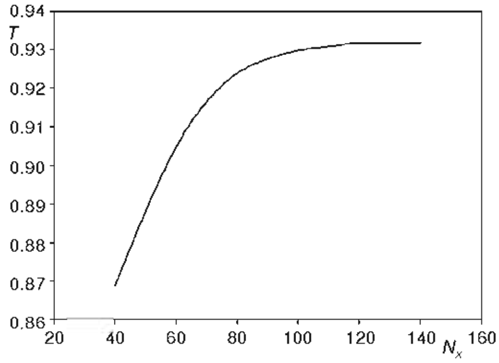

Figure 6. ***T*** **grid sensitivity study at** $x = 0.75\ L_x$, $y = 0$ **and** $t = 100$

where $1/\mathrm{Re}_{\mathrm{nf}} = \mu_{\mathrm{nf}}/\rho_{\mathrm{nf}} U_{\mathrm{in}} b_{1/2}$. The inlet mass flow rate is assumed constant and Reynolds number is corrected due to the nanofluid viscosity, where $1/\mathrm{Pr}_{\mathrm{nf}} = K_{\mathrm{nf}}/\mu_{\mathrm{nf}}(c_p)_{\mathrm{nf}}$ and $\mathrm{Pe}_{\mathrm{nf}} = \mathrm{Pr}_{\mathrm{nf}}\mathrm{Re}_{\mathrm{nf}}$.

The effective heat capacity is calculated with correlation as proposed by Pak *et al.* [37].

$$(c_p)_{\mathrm{nf}} = (1 - \varphi)(c_p)_{\mathrm{bf}} + \varphi(c_p)_{\mathrm{p}} \quad (20)$$

The effective conductivity is calculated using equation introduced by Yu *et al.* [21]:

$$K_{nf} = \left[\frac{K_{\mathrm{p}} + 2K_{\mathrm{bf}} + 2(K_{\mathrm{p}} - K_{\mathrm{bf}})(1+\beta)^3 \phi}{K_{\mathrm{p}} + 2K_{\mathrm{bf}} - (K_{\mathrm{p}} - K_{\mathrm{bf}})(1+\beta)^3 \phi} \right] K_{bf} \quad (21)$$

where $\beta = 0.1$ is used to calculate the thermal conductivity of nanofluid. For viscosity we use two experimental correlations proposed by Nguyen *et al.* [22]:

$$\frac{\mu_{\mathrm{nf}}}{\mu_{\mathrm{bf}}} = 1 + 0.025\phi + 0.015\phi^2 \quad \text{for } \mathrm{Al_2O_3}\text{-water}$$

and

$$\frac{\mu_{\mathrm{nf}}}{\mu_{\mathrm{bf}}} = 1.475 - 0319\phi + 0.051\phi^2 + 0.009\phi^3 \quad \text{for CuO-water}. \quad (22)$$

Result and discussion

Jet simulation

The case of 2-D forced jet is considered in the streamwise extent of $L_x = 25$. The Reynolds number is Re = 300. The Prandtl number is equated to 6.2 for pure water. The domain was discretized using 1000 points to represent the streamwise x extend of the domain and 526 points in the MG direction. A time step of 0.05 was used in this work.

For CuO-water

Figures 7 and 8 illustrate the relation between the velocity time history at $x = 0.5\ L_x$, and $y = 0$ and the solid volume fraction. The results show a decrease in the amplitude of velocity time history with any increase in the solid volume fraction. This is as a consequence of the decrease in the flow Reynolds number.

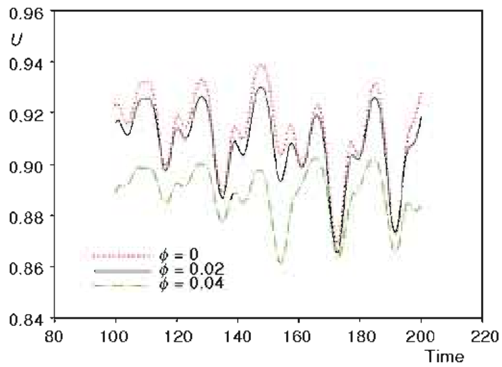

Figure 7. *U* velocity time histories at $x = 0.5L$ *and* $y = 0$ with different solid volume fraction for CuO-water

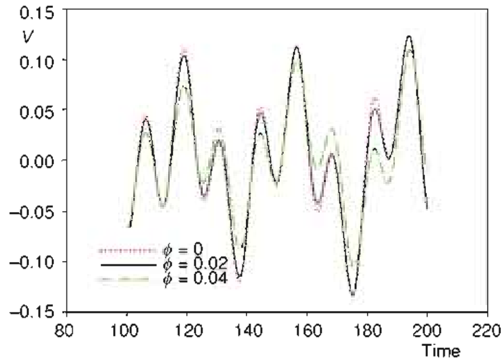

Figure 8. *V* velocity time histories at $x = 0.5L$ *and* $y = 0$ with different solid volume fraction for CuO-water

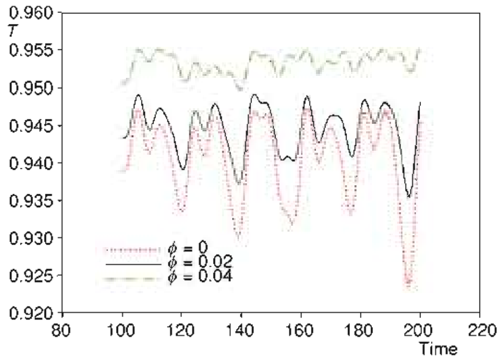

Figure 9. Temperature time history at $x = 0.5L$ and $y = 0$ with different solid volume fraction for CuO-water

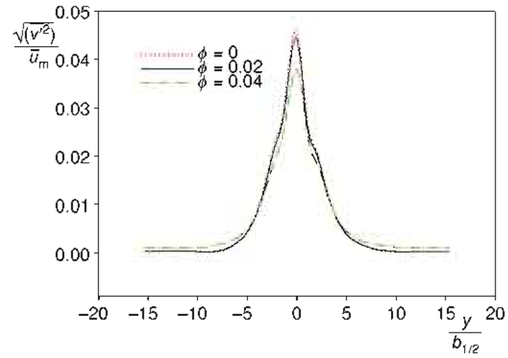

Figure 10. Turbulent intensity for $(\overline{v'^2})^{1/2}/\bar{u}_m$ at $x = 0.5L$ for CuO-water

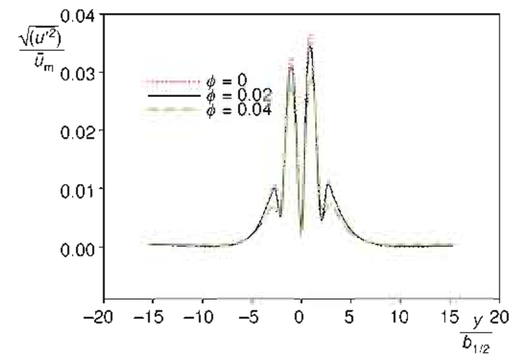

Figure 11. Turbulent intensity for $(\overline{u'^2})^{1/2}/\bar{u}_m$ at $x = 0.5L$ for CuO-water

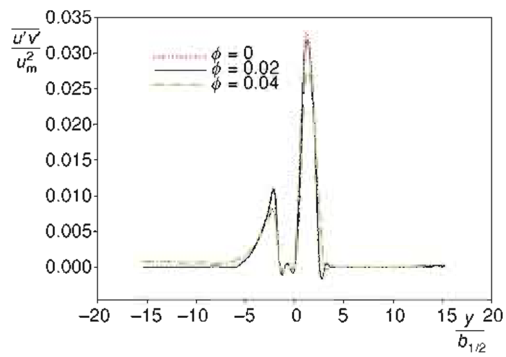

Figure 12. Reynolds stress for $\overline{u'v'}/\bar{u}_m^2$ at $x = 0.5L$ for CuO-water

Figure 9 indicates the relation between temperature time history at $x = 0.5\,L_x$ and $y = 0$, and the solid volume fraction. The result shows when the solid volume fraction increases the temperature amplitude temperature time history is decreased. Any decrease in Reynolds number and velocity amplitude cause a decrease in the temperature amplitude of history. Figures 10--12 show the turbulent intensities and Reynolds stress as a function of the solid volume fraction. Since the flow Reynolds number decreases as a consequence of the decrease in turbulent intensities and Reynolds stresses, the results indicate a decrease in turbulent intensities and Reynolds stress as the solid volume fraction is increased.

For Al_2O_3-water

Figures 13 and 14 illustrate the relation between the velocity time history at $x = 0.5\,L_x$ and $y = 0$, and the solid volume fraction. The results show a decrease in the amplitude of velocity time history when the solid volume fraction increased.

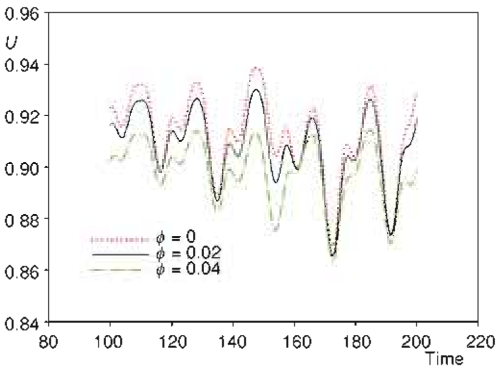

Figure 13. Velocity time history for the *U* component at *x* = 0.5*L* and *y* = 0 for Al_2O_3-water

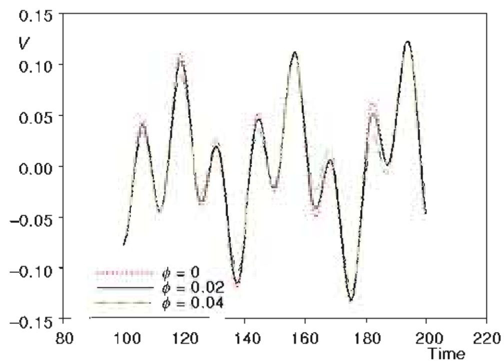

Figure 14. Velocity time history for the *V* component at *x* = 0.5*L* and *y* = 0 for Al_2O_3-water

Figure 15 indicates the relation between the temperature time history at $x = 0.5\,L_x$, $y = 0$, and the solid volume fraction. It shows a decrease in the amplitude of temperature time history as the solid volume fraction increases.

The velocity time history indicates that as the nanoparticle volume fraction increases, the amplitude of turbulence decreases. This causes an increase in the fluid viscosity and as a consequence decreases in the flow Reynolds number. For temperature time history any decrease in Reynolds number and the velocities amplitude cause a decrease in the amplitude of temperature time history.

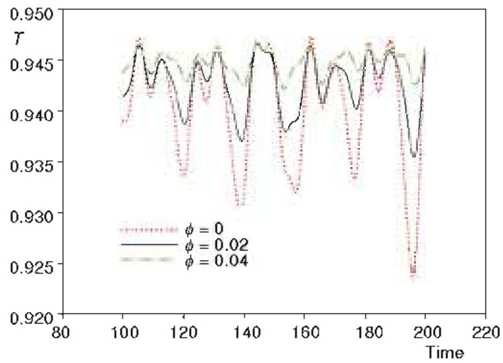

Figure 15. Temperature time history at *x* = 0.5*L* and *y* = 0 for Al_2O_3-water

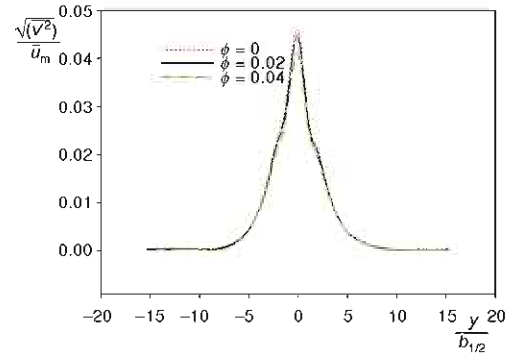

Figure 16. Turbulence intensity for $(\overline{v'^2})^{1/2}/\bar{u}_m$ at $x = 0.5L$ for Al_2O_3-water

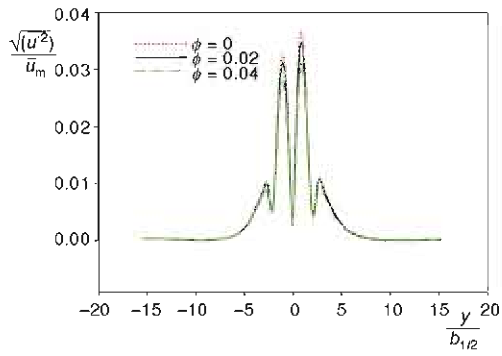

Figure 17. Turbulence intensity for $(\overline{u'^2})^{1/2}/\bar{u}_m$ at $x = 0.5L$ for Al_2O_3-water

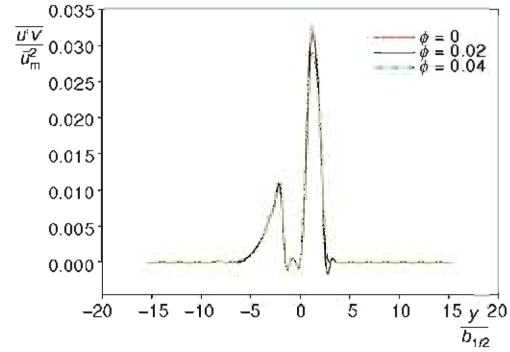

Figure 18. Reynolds stress for $\overline{u'v'}/\bar{u}_m^2$ at $x = 0.5L$ for Al_2O_3-water

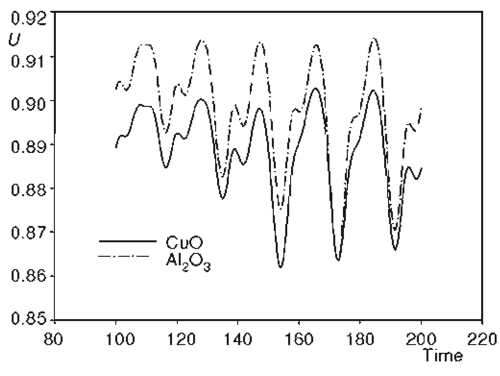

Figure 19. Velocity time history for the U component at $x = 0.5L$ and $y = 0$

Figures 16-18 show turbulent intensities and Reynolds stress as a function of the solid volume fraction. The results show a decrease in turbulent intensities and Reynolds stress as the solid volume fraction increases. The profile indicates that as the nanoparticle volume fraction increases, the turbulent intensities and Reynolds stress decreases. This is related to decrease in the flow Reynolds number.

Comparison of two different nanoparticles

In this section we compare the different results for both nanofluid with volume fraction of 0.04.

Figures 19 and 20 illustrate the variation of turbulence velocity amplitude for two different nanoparticles.

The Reynolds number with respect to any addition in CuO is less than that of Al_2O_3 nanoparticle. This is related to the effective viscosity which is greater when CuO is used than the effective viscosity when Al_2O_3 is employed. Thus the velocity amplitude of turbulence in Al_2O_3 water is greater than that of CuO-water.

Figure 21 shows the temperature amplitude of turbulence in CuO-water nanofluid which is greater than that in Al_2O_3-water nanofluid. This is explained owing to the increases in the peclet number when CuO-water is used instead of

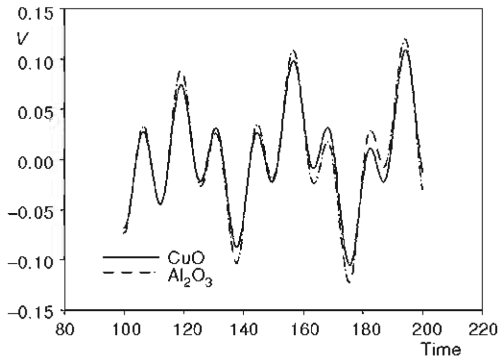

Figure 20. Velocity time history for the V component at $x = 0.5L$ and $y = 0$

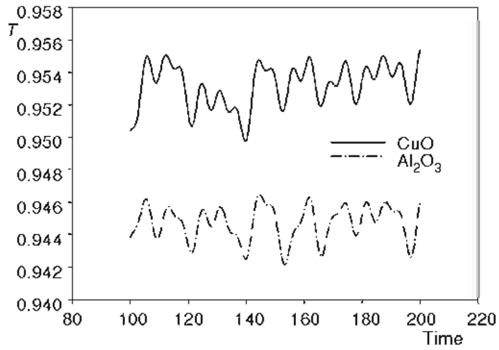

Figure 21. Temperature time history at $x = 0.5L$ and $y = 0$

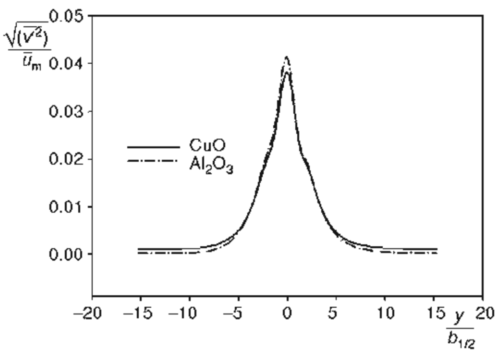

Figure 22. Turbulence intensity for $(\overline{v^2})^{1/2}/\overline{u}_m$ at $x = 0$

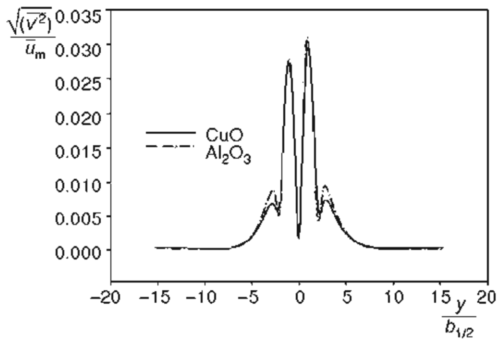

Figure 23. Turbulence intensity for $(\overline{u'^2})^{1/2}/\overline{u}_m$ at $x = 0.5L$

Al_2O_3-water. Figures 22-24 show the relation between the solid volume fraction and turbulent intensities and Reynolds stress. The Reynolds number with respect to any addition in CuO is less than the Reynolds number with any addition of Al_2O_3 nanoparticle. Thus the Reynolds stress and turbulence intensities in Al_2O_3-water is greater than the Reynolds stress in CuO-water.

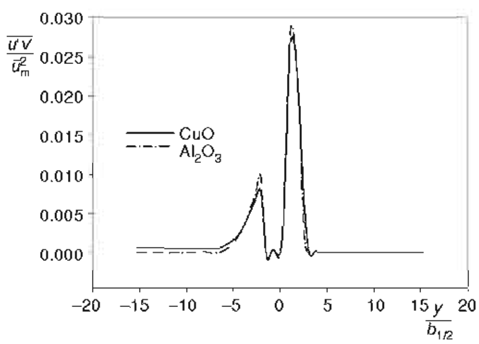

Figure 24. Reynolds stress for $\overline{u'v'}/\overline{u}_m^2$ at $x = 0.5L$

Conclusions

Direct numerical simulation of a 2-D incompressible spatially developing forced jet flow has been studied numerically for two different nanofluids in this work. A compact finite difference was used to represent the spatial derivatives in streamwise direction and a mapped compact finite difference method was used for derivatives in the MG direction. The simulations were time advanced by means of the third order Runge-Kutta method.

The results revealed a decrease in the amplitude of velocity and the temperature time history with any increase in the nanoparticle fraction. Results also indicate that the Reynolds stress and turbulence intensities were decreased with any increase in the solid volume fraction for both nanofluids. In addition a comparison is made between the results of Al_2O_3-water and CuO-water nanofluids. In CuO-water with any increase in ϕ the decrease in Reynolds number is much more pronounced than Al_2O_3-water. Thus the amplitude of velocity time history, turbulence intensities, and Reynolds stress in Al_2O_3-water is greater than that in CuO-water. In Al_2O_3-water with any increase in ϕ the decrease in Peclet number is much more experienced than CuO-water. Thus the temperature amplitude in CuO-water is greater than that in Al_2O_3-water.

Nomenclature

$b_{1/2}$ – half width jet, [m]
c – advection speed of the large-scale structures
c_p – special heat capacity, [$JKg^{-1}K^{-1}$]
K – conductivity coefficient, [$Wm^{-1}K^{-1}$]
N_x – direction x number of grid in
N_y – direction y number of grid in
Pe – Peclet number ($\rho Ub_{1/2}c_p/K$), [–]
Pr – Prantle number ($c_p\mu/K$), [–]
Re – Reynolds number ($Ub_{1/2}/\nu$), [–]
T – instantaneous temperature, [K]
t – time, [s]
U, V – instantaneous velocity, [ms^{-1}]
u, v – computational flow velocity component, [ms^{-1}]
x, y – Cartesian co-ordinate, [m]

Greek symbols

ζ – finite computational domain
λ – stretching parameter
μ – viscosity, [$Nm^{-2}s$]
ν – dynamic viscosity, [m^2s^{-1}]
ρ – density, [kgm^{-3}]
ϕ – nanofluid volume fraction
ψ – stream function
$\vec{\omega}(\omega_1, \omega_2, \omega_3)$ – rotational term in x, y, and z co-ordinate (= $\nabla \times$U)

Subscripts

bf – base fluid
c – computational
nf – nanofluid
p – nanoparticle
0 – base and initial temperature velocity
∞ – infinity

References

[1] Choi, S. U. S, Enhancing Thermal Conductivity of Fluids with Nanoparticles, *Developments and Applications of Non-Newtonian Flows, 231* (1995), 66, pp. 99-105
[2] Murshed, S. M. S., Leong, K. C., Yang, C., Thermo Physical and Electro Kinetic Properties of Nanofluids-A Critical Review, *Applied Thermal Engineering, 28* (2008), 17-18, pp. 2109-2125
[3] Maiga, S. E. B., *et al.*, Heat Transfer Behaviors of Nanofluids in a Uniformly Heated Tube, *Superlattices and Microstructures, 35* (2004), 3-6, pp. 453-462
[4] Maiga, S. E. B., *et al.*, Hydrodynamic and Thermal Behaviors of a Nanofluid in a Uniformly Heated Tube, in: Computational Studies, vol. 5, WIT Press, Southampton, UK
[5] Maiga, S. E. B., *et al.*, Heat Transfer Enhancement in Turbulent Tube Flow Using Al_2O_3 Nanoparticle Suspension, *International Journal of Numerical Methods for Heat and Fluid Flow, 16* (2006), 3, pp. 275-292
[6] Mirmasoumi, S., Behzadmehr, A., Numerical Study of Laminar Mixed Convection of a Nanofluid in a Horizontal Tube Using Two-Phase Mixture Model, *Applied Thermal Engineering, 28* (2008), 7, pp. 717-727
[7] Izadi, M., Behzadmehr, A., Jalali-Vahida, D., Numerical Study of Developing Laminar Forced Convection in an Annulus, *International Journal of Thermal Sciences, 48* (2009), 11, pp. 2119-2129

[8] Duangthongsuk, W., Wongwises, S., Heat Transfer Enhancement and Pressure Drop Characteristics of TiO_2-Water Nanofluid in a Double-Tube Counter Flow Heat Exchanger, *International Journal of Heat and Mass Transfer, 52* (2009), 7-8, pp. 2059-2067
[9] Behzadmehr, A., Saffar-Avval, M., Galanis, N., Prediction of Turbulent Forced Convection of a Nanofluid in Tube with Uniform Heat Flux Using a Two Phase Approach, *International Journal of Heat and Fluid Flow, 28* (2007), 2, pp. 211-219
[10] Chen, H., *et al.*, Heat Transfer and Flow Behavior of Aqueous Suspensions of Titanate Nanotubes, *Powder Technology, 183* (2008), 1, pp. 63-72
[11] He, Y., *et al.*, Heat Transfer and Flow Behavior of Aqueous Suspensions of TiO_2 Nanoparticles Flowing Upward through a Vertical Pipe, *International Journal of Heat and Mass Transfer, 50* (2007), 11-12, pp. 2272-2281
[12] Zeinali Heris,S., Etemad, S. Gh., Nasr Esfahany, M., Experimental Investigation of Oxide Nanofluids Laminar Flow Convective Heat Transfer, *International Communications in Heat and Mass Transfer, 33* (2006), 11, pp. 529-535
[13] Talebi, F., Mahmoudi, A. H., Shahi, M., Numerical Study of Mixed Convection Flows in a Square Lid-Driven Cavity Utilizing Nanofluid, *International Communication in Heat and Mass Transfer, 37* (2010), 1, pp. 79-90
[14] Shahi, M., Mahmoudi, A. H., Talebi, F., Numerical Study of Mixed Convective Cooling in a Square Cavity Ventilated and Partially Heated from the Below Utilizing Nanofluid, *International Communications in Heat and Mass Transfer, 37* (2010), 2, pp. 201-213
[15] Lee, J., Mudawar, I., Assessment of the Effectiveness of Nanofluids for Single-Phase and Two-Phase Heat Transfer in Micro-Channels, *International Journal of Heat and Mass Transfer, 50* (2007), 3-4, pp. 452-463
[16] Santra, A. K., Sen, S., Chakraborty, M., Study of Heat Transfer Due to Laminar Flow of Copper-Water Nanofluid through Two Isothermally Heated Parallel Plates, *International Journal of Thermal Sciences, 48* (2009), 2, pp. 391-400
[17] Nguyen, C. T., *et al.*, An Experimental Study of a Confined and Submerged Impinging Jet Heat Transfer Using Al_2O_3-Water Nanofluid, *International Journal of Thermal Sciences, 48* (2009), 2, pp. 401-411
[18] Luo, X. Y., Ying, A., Abdou, M., Numerical Study of MHD Effect on Liquid Metal Free Jet under Complex Magnetic Field, *Fusion Eng., 81* (2006), 8-14, pp. 1451-1458
[19] Konkachbaev, A., Morley, N. B., Abdou, M., Effect of Initial Turbulent Intensity and Velocity Profile on Liquid Jets for IFE Beam Line Protection, *Fusion Eng., 63-64* (2002), pp. 619-624
[20] Konkachbaev, A., Morley, N. B., Stability and Contraction of Rectangular Liquid Metal Jet in Vacuum Environment, *Fusion Eng., 51-52* (2000), pp. 1109-1114
[21] Yu, W., Choi, S. U. S., The Role of Interfacial Layers in the Enhanced Thermal Conductivity of Nanofluids: A Renovated Maxwell Model, *Journal of Nanoparticle Research, 5* (2003), 1-2, pp. 167-171
[22] Nguyen, C. T., *et al.*, Temprature and Particle-Size Dependent Viscosity Data for Water-Based Nanofluids-Hysteresis Phenomenon, *International Journal of Heat and Fluid Flow, 28* (2007), 6, pp. 1492-1506
[23] Schlichting, H., Boundary-Layer Theory, 8^{th} ed, Springer-Verlag, Berlin, 2000
[24] Satake, S., Kunugi, T., Direct Numerical Simulation of an Impinging Jet Into Parallel Disks, *Int.J.Numer. Meth. Heat Fluid Flow, 8* (1998), 7, pp. 768-780
[25] Pauley, L. R., Moin, P., Reynolds, W. C., The Structure of Two-Dimensional Sepration, *J.Fluid Mech, 220* (1990), pp. 397-411
[26] Maghrebi, M. J., Soria, J., Outflow Boundary Condition Issues in DNS of Three Dimensional Plane Wake Flow, *Journal of Aerospace Science and Technology JAST, 3* (2006), 4, pp. 177-183
[27] Maghrebi, M. J., Zarghami, A., DNS of Forced Mixing Layer, *International Journal of Numerical Analysis and Modeling (ijnam), 7* (2010), 1, pp. 173-193
[28] Lele, S. K., Compact Finite Difference Scheme with Spectral-Like Resolution, *Journal of Computational Physics, 103* (1992), 1, pp. 16-43
[29] Wray, A., Hussaini, M. Y., Numerical Experiments in Boundary Layer Stability, *Proc. R. Soc. Lond., A 392* (1984), pp. 373-389
[30] Stuart, J. T., On Finite Amplitude Oscillation in Laminar Mixing Layer, *JFM, 29* (1967), 03, pp. 417-440
[31] Abramovich, G. N., The Theory of Turbulent Jets, MIT Press, Cambridge, Mass., USA, 1963
[32] Van der Hegge Zijnen, B. G., Measurements of the Velocity Distribution in a Plane Turbulent Jet of Air, *Applied Scientific Research, 7* (1958), 4, pp. 256-276

[33] Thorne, K., Application of Classical Physics – Chapter 14: Turbulence. Caltech Lecture Course Ph136 (2004), http://www.pma.caltech.edu/Courses/ph136/yr2004
[34] Morchain, J., Maranges, C., Fonade, C., CFD Modelling of a Two-Phase Jet Aerator under Influence of a Crossflow, *Water Research, 34* (2000), 13, pp. 3460-3472
[35] Aziz, T. N., Raiford, J. P., Khan, A. A., Numerical Simulation of Turbulent Jets, *Engineering Applications of Computational Fluid Mechanics, 2* (2008), 2, pp. 234-243
[36] Shahi, M., Mahmoudi, A. H., Talebi, F., Numerical Modeling of Steady Natural Convection Heat Transfer in a 3-Dimensional Single Ended Tube Subjected to a Nanofluid, *International Communications in Heat and Mass Transfer, 37* (2010), 10, pp. 1535-1545
[37] Pak , B., Cho, Y., Hydrodynamic and Heat Transfer Study of Dispersed Fluids with Submicron Metallic Oxide Particles, *Experimental Heat Transfer, 11* (1998), 2, pp. 151-170

Paper submitted: October 11, 2010
Paper revised: January 15, 2012
Paper accepted: February 9, 2012